Precession electron diffraction and TEM applications

S. Nicolopoulos* , D.Bultreys

* Consultant IUCr Electron Crystallography Comission
NanoMEGAS SPRL, Blvd Edmond Machtens 79, B-1080 Brussels, Belgium
info@nanomegas.com , www.nanomegas.com

Abstract Despite its success in solving crystal structures, X-Ray diffraction has serious limitations to deal with nanostructures of nm size level. After the discovery of the precession electron diffraction by Vincent and Midgley and the introduction of dedicated precession electron diffraction devices to TEM microscopes, several nanocrystal structure determinations have been obtained so far. Recent new applications like precession 3D diffraction tomography , precession assisted 3D image tomography and (EBSD-TEM like) orientation phase mapping widen considerably the application field of TEM for electron crystallography.

Introduction

Crystal structure determination of a single crystal involves collection measurement of diffraction intensities and mathematical treatment (like direct methods) to solve the crystal structure **(FIG.1)** Diffraction intensities are defined as kinematic and there exist a simple relationship between structure factor F_{hkl} and (hkl) reflection's intensity. However, to study crystal structure of individual nanocrystals is only possible with transmission electron microscopy and not possible with single crystal or (or powder) X-Ray where the minimum crystal size is restricted to 5 microns (for Synchrotron single crystal experiments).On the other hand , in any TEM we can obtain a high resolution image of any nanoparticle as well its associated electron diffraction pattern in the back focal plane of the electron microscope **(FIG.2).**

Dynamical electron diffraction and precession electron diffraction

Although we can measure accurately electron diffraction (ED) intensities for any nanocrystal we cannot unfortunately use this information to solve its structure using the standard mathematical tools like in X-Ray diffraction.The reason is that electron interaction with matter is about 10^4 stronger than X-Rays and this results to strong dynamical scattering that may alter diffracted intensities so much that cannot be trusted for crystal structure refinement, unless crystal thickness is very thin (< 1 nm).This is why electron crystallography was not until recently routine structure identification tool like X-Ray crystallography **[1-2]** where beam-matter interactions are kinematical and structure factors can be directly derived from intensity data. For example in **FIG.2** (left) we can observe a clear example of how dynamical intensities of a rather thick sample (> 1 nm) are completely different from their ideal values-see simulated pattern on the right- and how space group extinctions are clearly violated in the "dynamical diffraction pattern", as intensities are clearly seen in places (red circles) where should be totally absent (like in X-Ray case).

Electron beam precession technique invented by Vincent , Midgley **[3]** in Bristol University (UK) gives a solution to this problem by increasing the kinematical character of the electron diffraction.This technique is equivalent to the X-Ray Buerger precession technique, where instead precessing the crystal (like in X-Ray precession) , electron beam is tilted and precessed on a cone surface having a common axis with the TEM optical axis.To obtain a stationary precession electron diffraction (PED) pattern instead of ring reflections **(FIG.2)** a simultaneous descan of the diffracted beam is realized by means of image shift TEM coils. As a result ofelectron beam precession, only few reflections are simultaneously excited in dynamical conditions and the resulting diffraction pattern can be considered close to kinematical or two beam conditions.In the resulting PED pattern kinematically forbidden reflections and multiple scattering are virtually eliminated (or greatly reduced) and space group identification can be easily done. By increasing precession angle **(FIG.3)** Ewald sphere covers bigger area in the reciprocal space and as a result more reflections are seen; at higher precession angle value (about 15-20 mrad) PED intensities change dramatically and become much closer to kinematical (X-Ray like) values **[4**].Maximum precession angles are related to maximum TEM dark field tilt angles and do depend on each particular TEM ;such maximum values usually range from 34-68 mrad (2-4°).

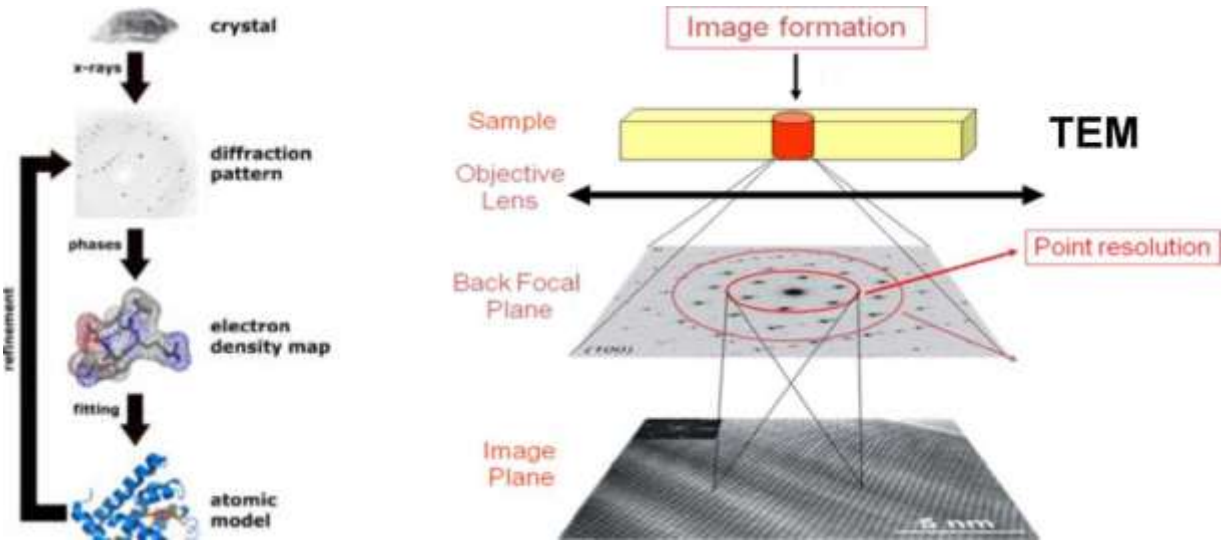

FIG.l (a) Schematics of crystal structure solution in X-Ray crystallography (b) schematics of image and diffraction in a transmission electron microscope (TEM)

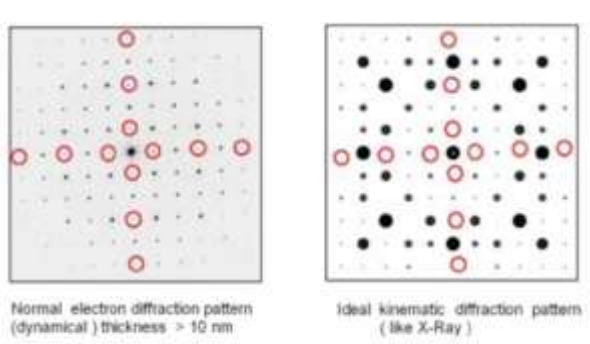

Scan and descan the beam to have stationary pattern

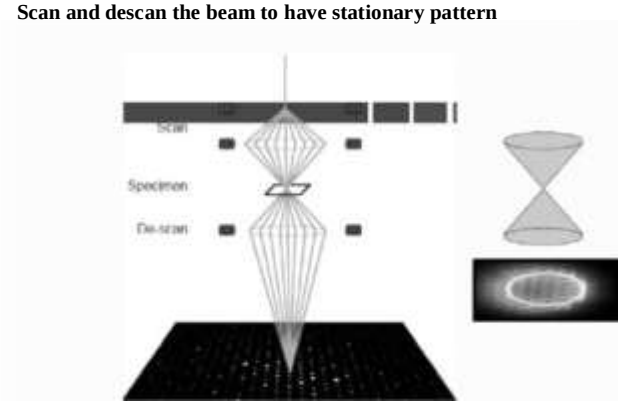

FIG.2 (left) [001] ED pattern of melilite mineral (a=b=7.8A c=5.0A S.G *P -4 2₁ m)* and simulated (kinematicel) ED pattern: red circles depict forbidden reflections that do appear in case of dynamical pattern (right) schematics of beam precession in a TEM

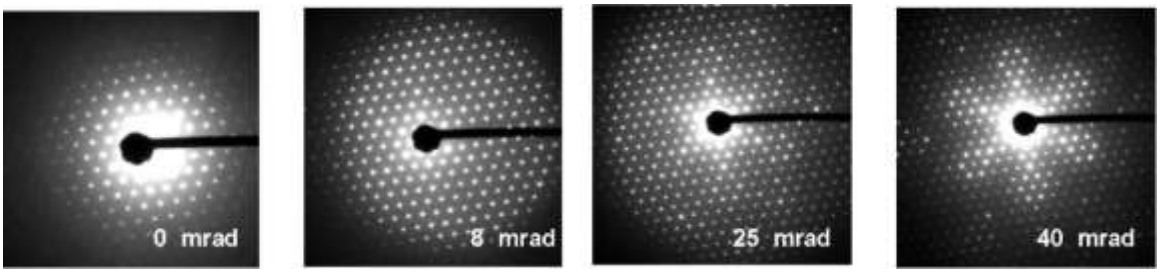

FIG.3 (left to right) [111] diffraction pattern of mayenite mineral (cubic a= 12.5 A) at different precession angles 0 mrad for complete dynamical pattern , 40 mrad precession angle quasi-kinematical electron diffraction pattern.

The first TEM precession interfaces have been developed by University teams in Oslo **[5,6],** Bologna **[7,8]** and by L.Marks , C.Own team in Northwestern University **[4]** ; however it was not until 2004 where our team in Brussels (ULB) developed **[9]** and supplied on a wide user basis precession systems (> 55 worldwide) able to retrofit in any modern TEM , when PED spread widely in many electron microscopy laboratories resulting in numerous publications and gaining recognition as innovative structure analysis technique in both TEM and X-Ray crystallographic communities **[10-18].** Precession devices (like the firstly developed "spinning star") and the latest digital version DigiSTAR **(FIG.4)** can be retrofitted to any modern TEM (like Tecnai 10-30 LaB6/FEG, Jeol 2100-2200 LaB6/FEG or the Zeiss Libra 120-200) or older TEM versions (like Philips CM 10-300 , Jeol 2000-2010 or Zeiss 912).PED device (hardware) can be plugged in the TEM electronic boards taking control of particular type of lenses: "beam tilt" (a pair of 4 lenses used for "beam scan") and "image shift" (a pair of 4 lenses used for "beam de-scan")."De-scanning" the beam is important to obtain a spot like PED pattern,otherwise patterns would have show circles-in place of ED spots-with diameter depending on precession angle **(FIG.2 right**).Precession frequency can vary from 0.2-2 kHz (high frequency as 100 Hz is requested for studying beam sensitive materials and to be used in combination with beam scanning applications- like ASTAR or ADT as will shown later).

Determination of space and point group symmetries with precession

One of the most straightforward applications of PED is symmery determination without need of CBED (convergent beam) information. By using PED the number of reflections present in the different Laue zones (LZ) increases strongly with increasing precession angle and it becomes easy to identify shifts and the periodicity difference between reflections located in those LZ. Shifts between observed LZ are related with Bravais lattice symmetry and observed LZ periodicity differences are related with presence (or not) of glide planes; such information can be used to identify possible space group symmetry of crystal without need of CBED.Morniroli et al **[14-17]** has shown how are related all different Laue classes/space & point group symmetries with observed ZOLZ/FOLZ in PED patterns. Visibility of ZOLZ/FOLZ is much greater when an TEM energy filter **[18]** is used **(FIG.5)**

Determination of crystal structures with precession

To solve 3D crystal structures we need a set of 3D hkl PED (quasi-kinematical) intensities, using the same mathematical procedures/software like in X-Ray diffraction for structure solution.There exist 3 main strategies from 3D electron diffraction data collection: a) data collected from different Zone Axis (ZA) patterns b)data collected with recently developed **ADT-3D (automatic precession diffraction tomography technique)** and c) data collected from ZA PED patterns in combination with powder X-Ray patterns.

In (a) approach a number of few (3 or more) ZA in a TEM **(FIG.6** Courtesy W.Cabrera MPI Dresden) is used and PED intensities can be measured automatically **[19]** from individual ZA on a CCD camera, image plate, photo film or high dynamic range detector (electron diffractometer **[11**]).A common scale factor is used between different ZA (to create a unique 3D hkl data set) having as reference the common intensity row between such ZA. Using direct methods software (like SIR2008 **[20])** or charge flipping algorithms **[21],** the 3D atomic structure model can be directly calculated having as input a list of 3D hkl PED intensity data set and a (usually minimum knowledge) of chemical formula and crystal symmetry (if not, structure determination can also be done in P1).Several structures could be solved ab-initio using that approach such as minerals **[22],** catalysts **[23**],complex oxide structures **[24,25,29]** and organic compounds (pharmaceuticals and proteins) **[26-28].** In all cases structure solution from PED data set clearly revealed all heavy and most of light atom positions like oxygens; attempts using conventional ED data sets were unable to provide any structure solution.

In (b) ADT-3D approach developed by U.Kolb **[30,31],** 3D hkl precession data are acquired through sequentially tilting a selected nanocrystal around an arbitrary crystallographic axis **(FIG.7)** with a variable tilt step down to 1° through the maximum TEM tilting range (usually from -45° to + 45°). Such a data set contains nearly all reflections present in the covered wedge of the reciprocal space.3D data acquisition can be done manually or automatically in some TEM platforms ; STEM ADT acquisition in nanobeam mode is especially effective for data collection from beam sensitive materials because it uses low dose illumination

FIG. 4 (left to right) Digital precession unit DigiSTAR and its interface with FEI T30 FEG (Mainz, Germany) and Zeiss Libra 200 Cs corrected, Zeiss SMT Oberkochen, Germany

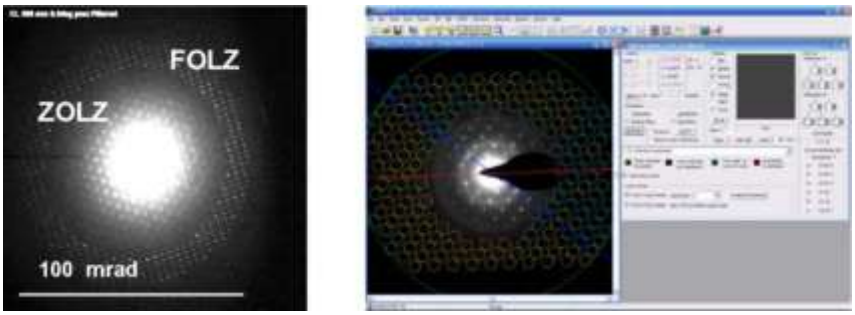

FIG. 5 (left) Libra 200 zero loss filtered PED pattern of mayenite mineral ; FOLZ reflections are clearly seen thanks to large 100 mrad angular range of the Omega filter.Comparison of symmetry of FOLZ and ZOLZ reflections allows to identify automatically point/ space group by *Space Group Determinator* software (right).

FIG. 6

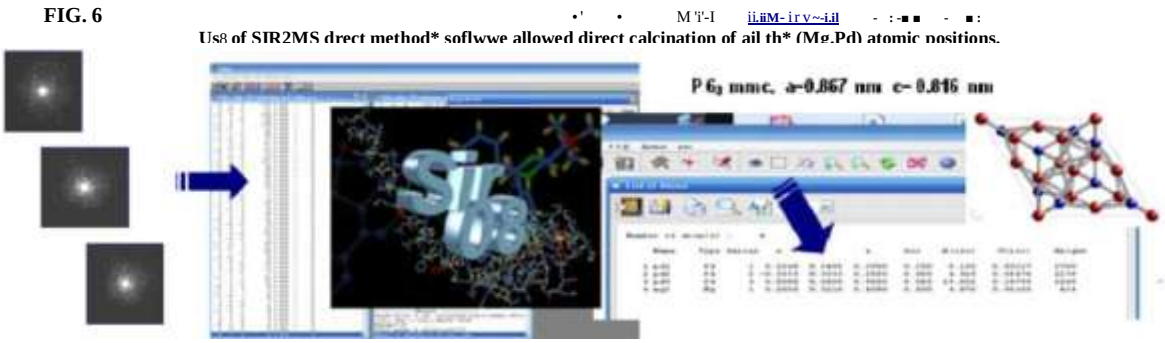

FIG.7 Reconstructed three dimensional reciprocal space showing hexagonal cell ($P6_3/mmc$ a= 0.396nm, c =0.536 nm) for NiTe nanocystal with data resolution up to 0.8A. Data have been collected from 80 precession diffraction patterns (precession angle 17 mrad) from -40° + 40° on Tecnai 30-FEG-STEM DigiSTAR (courtesy Dr.E.Mugnaoili, Dr.U.Kolb Mainz Univ)

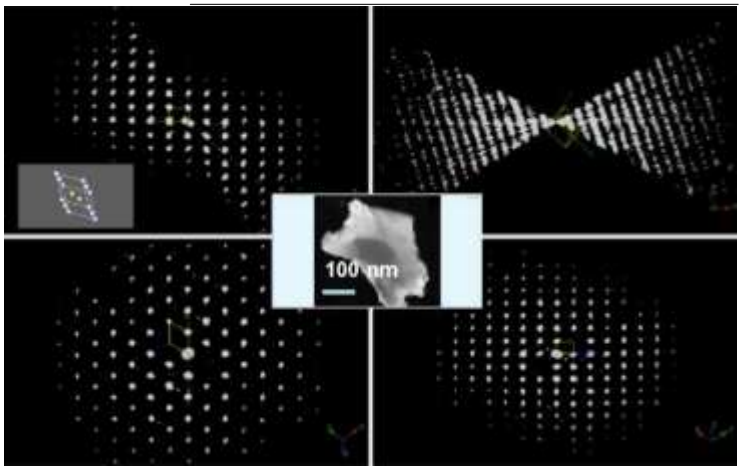

conditions in STEM.The advantage of ADT-3D data collection over individual ZA collection is that data collection can begin from any arbitrary (non-oriented) section of reciprocal space without any prior knowledge of the crystal cell ; after collection of typically 90 reciprocal space sections with single-tilt TEM holder , 3D reciprocal cell can be reconstructed automatically, crystal cell can be accurately determined (2-5% error) and 3D intensities can be measured to provide full 3D structure solution.Similar approaches for 3D data collection have been used recently also in **[32].**

In approach (c) we may combine PED TEM data with X-Ray powder diffraction data if available ; is known for instance that X-Ray powder techniques are currently used for standard ab-initio structure determination, however in many cases structure solution is not possible for several reasons : reflection overlap inherent to powder data, poor crystallization, peak broadening related to nm crystal size or existence of unknown polymorphs. Taking into account that X-Ray and electron scattering factors show similar trends with sin 8/X, strong and weak reflections in X-Rays are also observed as strong and weak quasi-kimematical PED reflections. Information coming from PED -TEM data can be very useful to estimate accurate individual *hkl* intensity contributions in case of overlapping X-Ray intensities **(FIG.7)** and can be combined with *hkl* reflections from *X-Ray* powder diffraction to accurately solve and refine *ab-initio* structures. This approach has been recently used to solve a complex TNU-9 **[33]** zeolite and unkownLi4Ti8Ni3O21 **[25]** structure in combination with Synchrotron X- Ray data.

Partial beam descan in PED patterns**[15]** or in LARBED technique (large angle rocking beam electron diffraction, that uses illumination tilt coils to sequentially change by software angle of incidence of electron beam over a large range) **[34]** delivers information about crystal symmetry, rocking beam information and could allow accurate structure factor determination on individual hkl ZA reflections. However, changing/control beam tilt by TEM-CCD software commands **[34,35]** is inherently slow (close or <1Hz) and applications are not compatible with beam scanning techniques like ADT or ASTAR phase/orientation mapping (see later).

Image BF (bright field) tomography and precession

Tomography (used to reconstruct the inside of an object as well as its external morphology) is a powerful tool to obtain 3D information from 2D projection images.In material sciences, the combination of both the HAADF-

STEM (sensitive to the atomic number) with electron tomography technique has demonstrated its capability to solve the 3D morphology of nanostructures avoiding the problems related with the diffraction contrast, present in conventional TEM mode imaging.Electron Tomography in BF-TEM has associated some problems for crystalline specimens : coherent Bragg diffraction at certain tilt angles, so the intensity of the projections changes in a non-monotonous way during the tilt process. Difficulties in 3D defect reconstruction includes thickness fringes, bend contours and strain fields related contrast .Using the combination of both tomography and precession techniques in the TEM microscope it is possible to obtain projections less affected with dynamical contrast **(FIG.9).** Electron beam precession in BF TEM mode leads to from quasi-two beams to strong two beams condition and extinction of bend contours related contrast. The viability of the combination of these two techniques has strong potential for defect reconstruction in BF-DF-TEM applications as an alternative to STEM-HAADF **[36]**

Precession and TEM phase -orientation imaging (EBSD-TEM like)

Electron backscatter diffraction (EBSD) technique of scanning electron microscopy (SEM) has gained popularity over the last decade as it provides an effective tool for the characterization of bulk crystalline materials with crystal phase and orientation maps with a resolution of up to 50 nm (FEG-SEM).In order to adress high resolution TEM orientation imaging needs for nanostructure materials characterization, we have developed a novel (Patent pending) **[37,38]** technique in collaboration with INP-CNRS Grenoble. ED/PED spot patterns are collected sequentially with a dedicated external (CCD) camera while the sample area (that is typically tens of square micrometers) is scanned by the primary electron beam and simultaneously precessed around the optical axis of the microscope **(FIG.10).** The tool named "ASTAR" (automatic TEM phase-orientation mapping) includes precession device "DigiSTAR" and dedicated scan generator such TEM does not need to possess its own scanning facility as "ASTAR-DigiSTAR" includes a dedicated scan generator. The external dedicated "fast" CCD camera (8 bit, > 150 frames/s, 250 x 250 pixels image size) is mounted in front of the TEM screen. During the scanning and precessing of the primary electron beam, thousands of PED spot patterns are recorded and stored in a computer's memory.

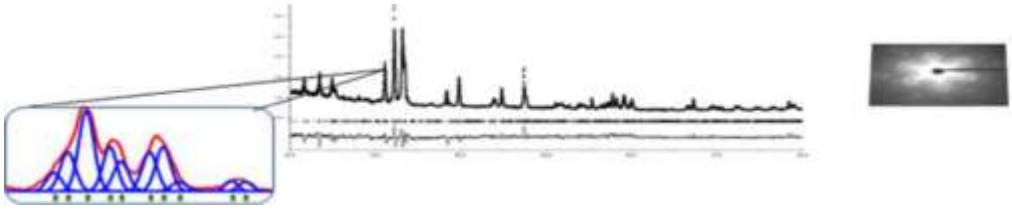

FIG. 8 Typical Syncrotron X-Ray powder diffraction pattern where reflection overlapping occurs in many reflection peaks.Information coming from TEM-PED patterns (upper right) can be very useful identifying correct individual reflections intensity

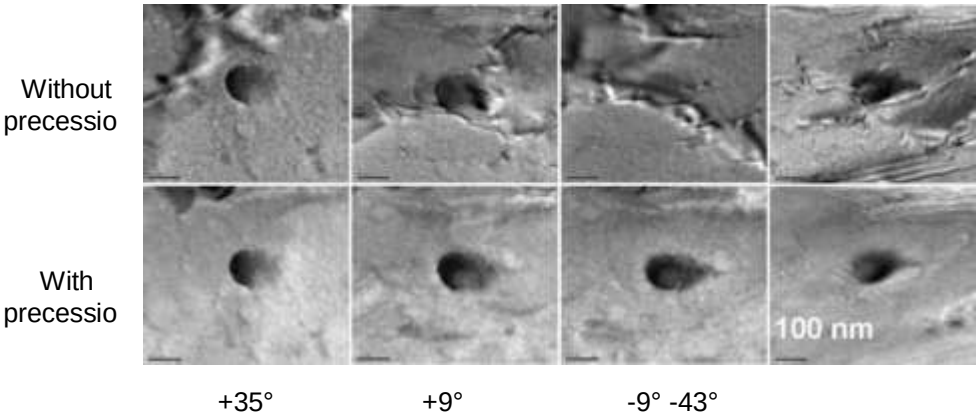

FIG.9 Bright field TEM tomography acquisition combined with beam precession (alternatively on/off) : Al thin foil with Sn precipitates, tilt series: +49° > a > -61°, angle step: 2°, Precession angle: 0.6° , magnification 25.000 x (Jeol 2100 -DigiSTAR) courtesy Rebled, Yedra,Portillo, Estrade, Peiro Univ Barcelona (Spain)

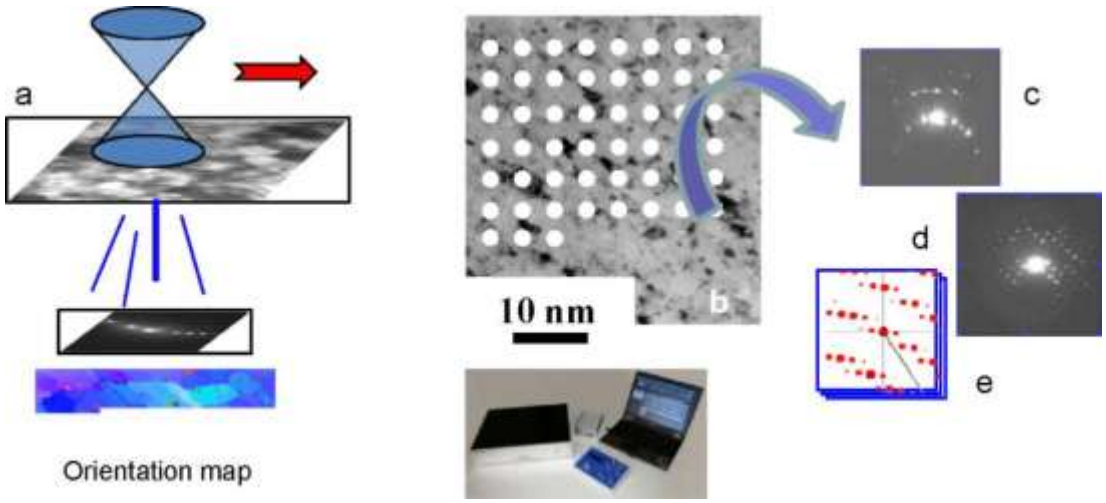

FIG.10 Schematics of the ASTAR beam scanning mode combined with precession diffraction (a), beam scanning over the sample (b) and generation of ED (c) or PED (d) patterns ; generation of simulated ED templates (e)

In order to proceed with nanocrystal orientation and phase identification of each experimental PED spot pattern, thousands of simulated ED spot patterns (so called templates) are utilized for each crystallographic phase in the sample **(FIG.11).** Local crystal orientations are obtained by comparing individually obtained PED spot patterns via cross-correlation matching techniques with pre-calculated ED templates generated every 1° (orientation resolution).For a typical map of 500x500 pixels, beam scanning (and precessing) over the sample area may take only 5-10 minutes. Comparison with simulated templates can be done off-line and may take about 5 minutes for highly symmetric cubic materials and 3-6 times longer for unit cells with lower symmetry as more templates must be generated.Template generation is done on the basis of inputs of the crystal structure parameters of the known phases (for with the spatial distribution is to be mapped) to the software. Typical mapped areas are of the order of 5x 5 microns; spatial resolution is about half the primary electron beam size, e.g. 10 nm for 20 nm spot size of a TEM/LaB_6 and can be as small as 1 nm for TEM-FEG microscopes **(FIG.12).**

FIG.12,13 show experimental crystal orientation and phase maps for different materials (metals nanoparticles, semiconductors **[39]**). Phase identification is done with cross-correlation and statistical match of experimental ED/PED pattens with generated ED templates of all possible (known) phases. Although the orientation and phase mapping coupled with template matching can work for some materials without using beam precession , there can be important limitations to the resulting quality of experimental ASTAR maps due to the intrinsic poor quality of experimentally acquired ED spot patterns. This might be the case for thicker crystals where ED patterns may show a combination of a strong diffuse inelastic scattering background, Kikuchi lines and fainter diffraction spots.Using precession diffraction (0.2-0.8°) in combination with sample area scanning , resulting PED patterns are of much superior quality than ED patterns as PED suppresses Kikuchi lines and other crystal thickness related effects; moreover PED patterns possess an increased number of observed ED spots with respect to standard (zero-precession-angle) ED spot patterns. As a consequence resulting matching correlation with simulated templates leads to much higher quality (noise and artifacts free) orientation and phase maps with precession**(FIG.14-17**).Using scanning and precession modes in ASTAR also generates PED patterns with FOLZ reflections visible and this helps to distinguish "subtle" differences between structures with same crystal cell parameters and symmetry,but different space groups (example mayemite-magnetite crystals **(FIG.15).**
We have also found that ASTAR combined precession helps to solve in orientation maps the well known 180° ambiguity **[40].** This ambiguity in the indexing of ED spot patterns arises from the fact that a particular diffraction spot may be indexed as either (hkl) or (-h-k-l). Using PED is helpful as FOLZ reflections may appear and lead to establish unambiguous orientation **(FIG.16**).As an example, **FIG.17** observation of austenite in ferrite grains in maps that were based on data that were acquired without precession are revealed to be artifacts related with 180° ambiguity and are effectively removed by using a small 0.5° precession angle.
A very exciting and promessing application of ASTAR precession based technique is orientation mapping for organic crystals **(FIG.18).** For such beam sensitive materials, it has been attempted to scan the area the specimen at a sufficiently high speed to capture diffraction information before irradiation damage may prevent the acquisition (TRIS structure C_{16} H_{48} N_4 O_{12}) and demonstrates that it is possible to collect relevant information without using cryo mode.
Again,it is important to stress that ASTAR-DigiSTAR can be retrofitted to any TEM (also the dedicated CCD camera can be transferred from one TEM to another) .

Conclusion
Besides the early work in solving structures with electron diffraction and HREM-TEM processing image techniques **[1-2,41]** it was only until recently with the wider availability of precession diffraction devices in different TEM that the interest for electron crystallography has been strongly reemerged worldwide.Using PED is possible to solve ab-initio crystal nanostructures, perform 3D BF image reconstruction artifact-free and create nm resolution EBSD-TEM like orientation/phase maps.Novel applications like structure determinations with energy-filtered PED **[18,42**],new algorithms for structure determination with PED and software for electron crystallography **[43,44],** theoretical research about PED intensity behaviour **[45,46]** and texture maps on organic structures (see text) are just a few examples of the rapidly expanding field of electron crystallography with PED.

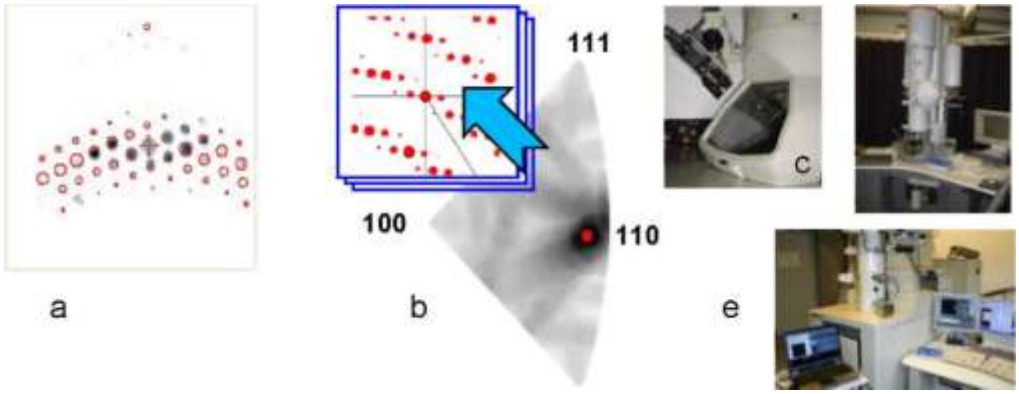

FIG.11 ASTAR : (a) experimental PED pattern is compared with each pre-calculated template in order to find the best match. (b) corresponding set of correlation indices may be plotted into the symmetry invariant section of the stereographic projection of the corresponding crystal phase , where darkest area indicates most probable symmetry orientation (c) High speed ED pattern collection (100 frames/s) dedicated CCD camera attached to the TEM (e) ASTAR-DigiSTAR interfaced at FEI Tecnai 20 F, Portland State Univ USA and JEOL 2200 FS at Humboldt Univ , Berlin, Germany

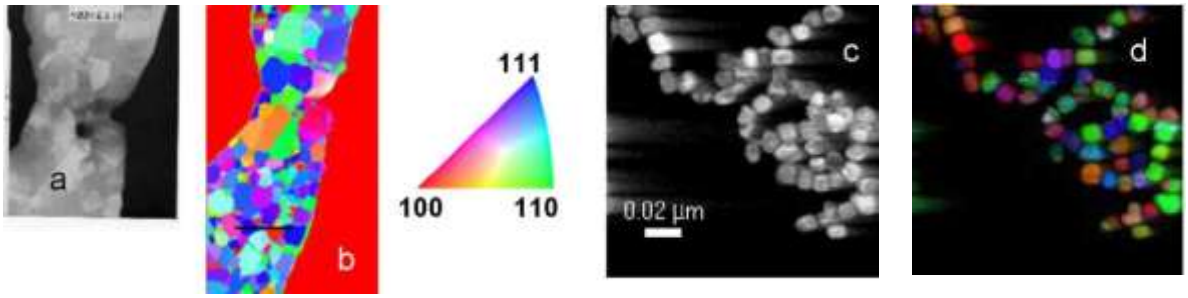

FIG.12 Bright field TEM image of Al thin foil after tensile stressing (a) and ASTAR orientation map (b) CM20 UTWIN ,8nm map resolution, Courtesy Dr.S.Godet ULB Brussels (c) bright field of Pt nanoparticles (5-50 nm diameter) and (d) ASTAR orientation map (1 nm resolution), precession angle 0.5°, JEOL 2010 FEG Courtesy Prof. P.Ferreira, J.Ganesh, Univ of Texas at Austin ,USA

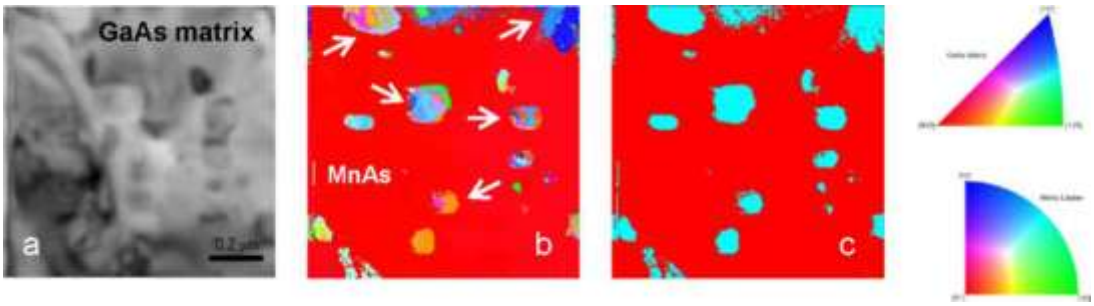

FIG.13 MnAs crystallites embedded on a GaAs matrix (a) [001] plan view TEM bright field image (b) ASTAR orientation map where MnAs crystallites are clearly seen - colours correspond to invese pole figure on the right c) ASTAR phase map where MnAs crystals are revealed as orthorombic phase after cross-correlation comparison with both hexagonal and orthorombic templates. Red backround color in b,c stands for [001] orientation of GaAs wafer . JEOL 2200 FS, precession angle 0.8°,Humboldt Univ Berlin, courstesy Dr. H.Kirmse, Dr. I.Hausler

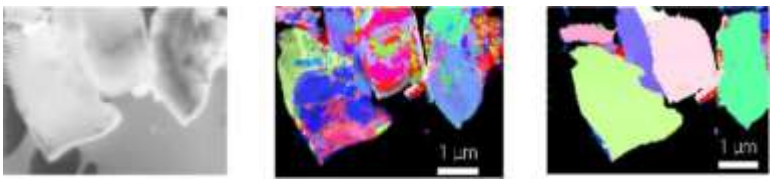

FIG.14 (a) mayenite crystallite virtual bright field image (b) orientation map created with ASTAR without using precession (c) accurate orientation map of the same area using a precession angle of **0.35°.** Colours correspond to inverse pole figure in FIG.14d.

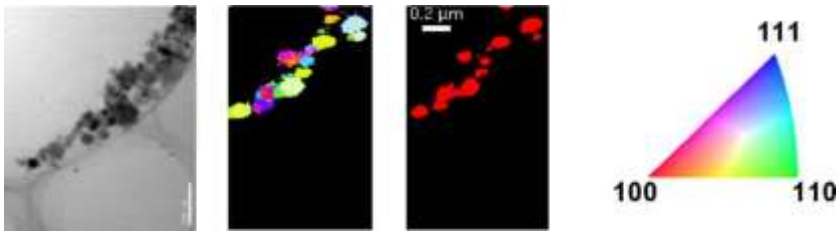

FIG.15 (a) Bright field TEM image a mixture of iron oxide nano-crystals of magnetite (Fe_3O_4,Fd3m,a= 0.832 nm) and maghemite (y-Fe_2O_3,$P4_132$, a = 0.833 nm) (b) ASTAR orientation map (c) ASTAR phase map revealing that crystals belong only to magnetite phase, FEI Tecnai 20F, precession angle of **0.3°** Portland State Univ USA, Courtesy Prof. P.Moeck

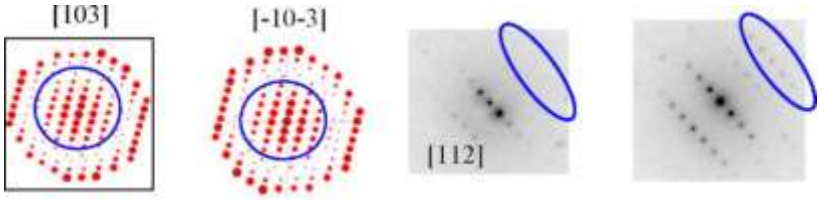

FIG.16 (a) Copper crystal ZOLZ ED pattern close to [103] may be indexed in two different ways that differ only by an azimuthal rotation around the zone axis by 180° (b) and (c). This indexing ambiguity can be overcome by using reflections from the first order Laue zone (FOLZ). Using the ASTAR precession diffraction mode, FOLZ reflections become visible. Compare (d) where the [112] zone axis pattern shows no visible FOLZ reflections, while there is an extra row of FOLZ reflections clearly visible in (e) as a result of 0.5° precession.

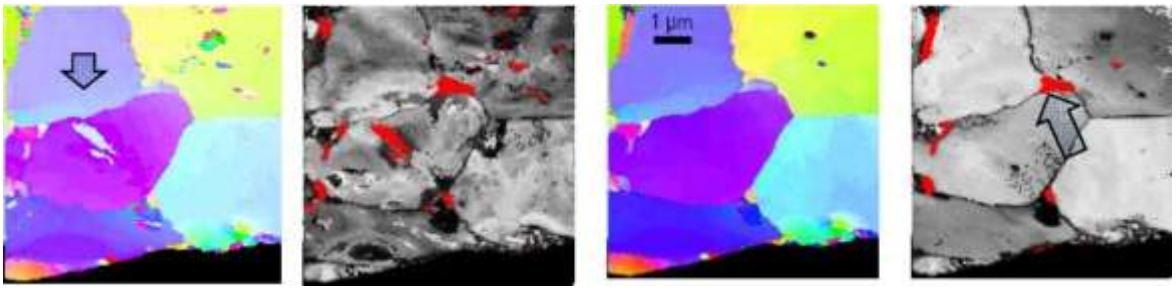

FIG.17 TRIP ferritic (bcc) steel (matrix) containing austenite fcc inclusions: ASTAR orientation map (a), crystal phase map, (b) superimposed on the reliability map (no precession) showing orientation and phase artifacts (see arrow) caused by the 180° indexing ambiguity; Orientation map (c) and crystal phase map superimposed on the reliability map (d) recorded from the same sample area with 0.5° precession. As a result of the ASTAR precession mode, the phase and orientation maps are showing correctly retained austenite phases (red color) only at the grain boundaries. Philips CM120, courtesy E. F. Rauch, M. Veron, SiMaP Grenoble, France.

FIG.18 (a) ASTAR orientation map of TRIS organic nanocrystal (Pna2$_1$ a=0.7768 , b=0.8725 c= 0.8855 nm ,C_{16} H_{48} N_4 O_{12}) Hundreds of electron diffraction patterns (b) were collected and automatically indexed (c) during beam scanning over the whole crystal area. The solutions are selected among the full set of possible pre-calculated templates (d) best matched solution is shown in the stereographic projection (spot size 15 nm NBD mode Jeol 3010 TEM , Courtesy M.Veron, E.Rauch, SIMAP Grenoble), WL Ling, J.Otero IBS Grenoble

REFERENCES

[I] BK Vainstein , Structure Analysis by Electron Diffraction Pergamon, New York 1964
[2] D.Dorset, Structural Electron Crystallography Plenum Press 1995
[3] Vincent R.,Midgley P.,Ultramicroscopy, 1994, 271-282.
[4] Own, C. S.: *PhD thesis*, System Design and Verification of the Precession Electron Diffraction Technique, Northwestern University, *2005*,*http://www.numis.northwestern.edu/Research/Current/precession.shtml*
[5] J.Gjonnes,V.Hansen, BS Berg, P.Runde, YF Gheng, K.Gjonnes,DL Dorset ,C.Gilmore Acta Cryst (1998) A54, 306-319
[6] BS Berg,V.Hansen, PA Midgley, J Gjonnes *Ultramicroscopy* **74** (1998) 147-157
[7] M Gemmi , L.Righi ,G.Calestani, A.Migliori, A.Speghini, M.Santarosa , M.Bettinelli *Ultramicroscopy* **84** (2000)133-142
[8] M.Gemmi, X.Zou, S.Hovmoller, A.Migliori, M.Vennstrom, Y.Anderson Acta Cryst A (2003) A59, 117-126
[9] www.nanomegas.com
[10] Weirich T., Portilo J., Cox G., Nicolopoulos S., Ultramicroscopy 106 (2006),164-175.
[I I] S.Nicolopoulos, A.Kuligin, K.Kuligin, K.Boulahya, G.Lepeshov, JL DelPlancke, A.Avilov , M.Nickolskiy,A.Ponce Electron Crystallography NATO Science Series Edited by T.Weirich, J.Labar and Xiaodong Zou Springer 2006 p.169-183
[12] Ultramicroscopy Vol.107, Issue 6-7,June 2007 New Fronteers in Electron Crystallography Guest Editors S.Nicolopoulos, TE Weirich
[13] A.Avilov , K.Kuligin, S.Nicolopoulos, M.Nickolskiy, K.Boulahya, J.Portillo, G.Lepeshov, B.Sobolev,JP Collette, N.Martin, AC Robins, P.Fischione Ultramicroscopy 107 (2007),431-444
[14] J. P. Morniroli, A. Redjaimia and S. Nicolopoulos, *Ultramicroscopy* **107** (2007) issue 6-7,514-522
[15] J. P. Morniroli, P.Stadelmann, G.Ji, S.Nicolopoulos Journal of Microscopy 2010
[16] J. P. Morniroli, G.Ji Mater Res Symp Proc Vol 1184 , 2009
[17] J. P. Morniroli, A. Redjaimia Journal of Microscopy Vol 227, pt 2 2007, p 157-171
[18] S.Nicolopoulos, D.Bultreys, G.Benner, H.Niebel, G.Pavia, M.Gemmi, B.Janssens M&M 2010 Proceedings Portland USA
[19] S.Hovmoller Ultramicroscopy 41 :121-135 , 1992
[20] Burla MC , Caliandro R., Camalli M., Carrozzini B., Cascarano GL., De Caro L., Giacovazzo C., Polidori G.,Siliqi D., Spagna R. J. Appl Cryst 40, 609-613 (2007)
[21] Palatinus, L.& Chapuis G. (2007) J. Appl.Cryst. 40, 786-790
[22] M. Gemmi and S. Nicolopoulos, *Ultramicroscopy* **107** (2007) issue 6-7,483-494
[23] Dorset D., Gilmore C. ,Jorda JL.,Nicolopoulos S., Ultramicroscopy **107** (2007) issue 6-7,462-473
[24] K.Boulahya, LR.Gonzalez, M.Parras, JMG Calbet, MS Nickolskiy, S.Nicolopoulos Ultramicroscopy 107(2007)431-444
[25] M.Gemmi, H.Klein, A.Rageau, P.Strobel, F LeGras Acta Cryst B66 (2010)
[26] D.Gueorguieva PhD Thesis Electron Cryst of 3D protein crystals Leiden 2008
[27] DG Guorguieva , L.Jiang, HW Zandbergen, S.Nicolopoulos, JP Abrahams EMC2008 Aachen vol 1, p.759-760
[28] EG Bitchell, MD Eddleston, CA Merill , W.Jones , PA Midgley EMC 2008, Vol.I p. 117-178
[29] P.Boullay,V.Dorcet, O.Perez, C.Grygiel,W.Prellier, B.Mercey,M.Hervieu, Phys. Rev B79, 2009,
[30] U. Kolb, T. Gorelik, M. T. Otten, *Ultramicroscopy* 2008, 108, 763-772.
[31] E. Mugnaioli, T. Gorelik, U. Kolb, *Ultramicroscopy* 2009, 109, 758-765
[32] D.Zhang, P.Oleynikov, S.Hovmoller, X.Zou Z. Kristalogr. 225 (2010) 94-102
[33] D.Xie, C.Baerlocher , L.McCusker J.Applied Cryst 2008, 41, 1115-1121
[34] C.Koch Utramicroscopy 2011 in press
[35] D.Zhang, D.Gruner , P.Oleynikov, W.Wan, S.Hovmoller, X.Zou Ultramicroscopy 111(2010) 47-55
[36] JM. Rebled, Ll. Yedra, J. Portillo, S. Estrade , F. Peiro Ultramicroscopy (2011) to be published
[37] E.F. Rauch et al., *Microsc. Microscopy and Analysis*, Issue 93, November (2008), S5.
[38] E.F. Rauch , J.Portillo,S.Nicolopoulos, D.Bultreys, S.Rouvimov, P.Moeck *Zeits. Krist.* 225, (2010) issue 2-3, 103-109.
[39] I.Hausler, D.Bultreys,E.F.Rauch, K.Volz,W.Neumann ICM17 Proceedings 2010 , Rio de Janeiro Brazil
[40] Champness, P. E.: Electron Diffraction in the TEM, BIOS Scient Publ Ltd, Oxford, 2001 ,Vo. 47, pp. 35-36.
[41] DL Dorset , S.Hovmoller , X.Zou Eds Kluwer Academic Publishers , Dordrecht 423-426 1997
[42] JG Kim , K. Song, K.Kwon, K.Hong, YJ Kim Journal of Electron Microscopy 1-11 (2010)
[43] G. Cascarano BEA algorithm for PED : School on Electron Crystallography Oct 29-30 2010 Daejeon S.Korea
[44] www.calidris-em.com // www.analitex.com // http://cime.epfl.ch/page-26784-en.html
[45] C.S.Own, L.D.Marks, W.Sinkler Acta Cryst A62 , 2006, 434-443
[46] J. Ciston, B. Deng, L.D. Marks, C.S. Own, W. Sinkler, *Ultramicroscopy* **108** (2008) 514-522